Near-Zero Thermal Expansion and High Ultraviolet Transparency in a Borate Crystal of $Zn_4B_6O_{13}$

Xingxing Jiang, Maxim S. Molokeev, Pifu Gong, Yi Yang, Wei Wang, Shuaihua Wang, Shaofan Wu, Yingxia Wang, Rongjin Huang, Laifeng Li, Yicheng Wu, Xianran Xing,* and Zheshuai Lin*

Zero thermal expansion (ZTE) crystals can retain a constant size in a specified temperature range, which challenges the common sense of the basic laws of physics that an object will always expand on heating and contract on cooling. ZTE crystals have been applied in many scientific and technical fields, such as high-precision instruments, protection shields for inflammables and explosives, and catalyst supports, where a high dimensional stability for resisting temperature change is required.[1–4] The search for the ZTE crystals is one of the most important issues in the investigation of materials with anomalous thermal

X. Jiang, P. Gong, Y. Yang, Prof. Y. Wu, Prof. Z. Lin
Center for Crystal R&D
Key Lab of Functional Crystals and Laser Technology
of Chinese Academy of Sciences
Technical Institute of Physics and Chemistry
Chinese Academy of Sciences
Beijing 100190, China
E-mail: zslin@mail.ipc.ac.cn
X. Jiang, P. Gong, Y. Yang, Prof. Z. Lin
University of Chinese Academy of Sciences
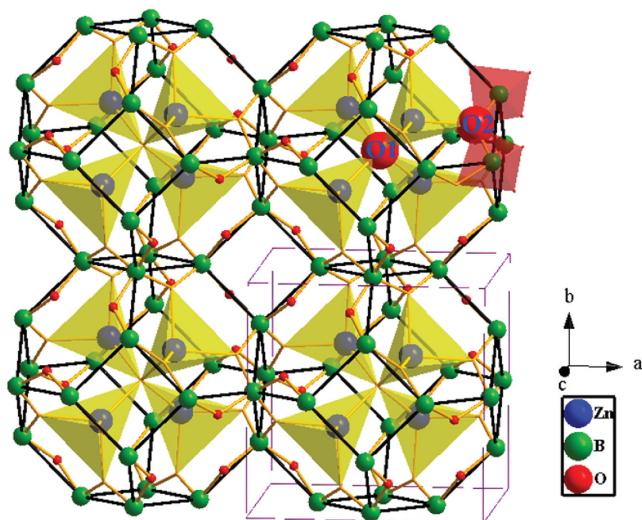Beijing 100049, China
Dr. M. S. Molokeev
Laboratory of Crystal Physics
Kirensky Institute of Physics
SB RAS
Krasnoyarsk 660036, Russia
Dr. M. S. Molokeev
Department of Physics
Far Eastern State Transport University
Khabarovsk 680021, Russia
W. Wang, Dr. R. Huang, Prof. L. Li
Key Laboratory of Cryogenics
Technical Institute of Physics and Chemistry
Chinese Academy of Sciences
Beijing 100190, China
S. Wang, Prof. S. Wu
Fujian Institute of Research on the Structure of Matter
Chinese Academy of Sciences
3

,[8] $Fe[Co(CN)_6]$,[9] TaO_2F,[10] $N(CH_3)_4CuZn(CN)_4$,[4] $YbGaGe$,[11] and $ZrMgMo_3O_{12}$.[12] However, due to d–d transitions of transition metals or the existence of heavy elements, the shortest optical absorption edges of these crystals are located just in the visible region, which seriously hinders their applications in ultraprecise optical instruments, which often operate in the ultraviolet (UV) region. [13] At the same time, for practical application purposes, the ZTE effect in crystals should be 3D isotropic, which could result in advantages such as ease of fabrication and manipulation, freedom from interface and local stress, and no occurrence of microcracks in the material during the thermal cycles. This suggests that the ideal ZTE crystal should crystallize in a cubic space group. However, among the previously reported intrinsic single-phase ZTE materials, only $Fe[Co(CN)_6]$,[9] TaO_2F,[10] and $N(CH_3)_4CuZn(CN)_4$[4] crystallize in a cubic crystal system. The exploration of intrinsic single-phase isotropic ZTE crystals remains a great challenge in thermally functional materials.

Borate crystals have attracted our attention because their shortest absorption edges are often down to the UV region. [14] For instance, β-BaB_2O_4 (BBO) and LiB_3O_5 (LBO) are widely used as the key devices for UV laser generation.[14] More importantly, borate crystals are suitable for ZTE exploration because their structures contain the typical features for anomalous thermal expansion.[15,16] A boron atom can be threefold or fourfold coordinated with oxygen atoms to form the $[BO_3]$ triangle or the $[BO_4]$ tetrahedron. These microscopic groups are strongly covalent and the bond lengths and angles remain almost constant as the ambient temperature varies.[15] Further interconnections of the rigid B–O groups can construct 1D, 2D, or 3D frameworks with a large structural diversity, in which rotation between the B–O groups may result in the anomalous thermal expansion.[15,16] Many borates, such as LBO,[16] $KBe_2BO_3F_2$,[17] $LiBeBO_3$,[18] $KZnB_3O_6$,[19] and $CsSiB_2O_6$[20] exhibit the anomalous-thermal-expansion (negative-thermal-expansion (NTE)) effect. However, the 3D ZTE effect has not yet been discovered in borates.

In order to search the 3D ZTE materials in borates, we propose to introduce cations with relatively large electronegativity into the 3D B–O framework with cubic symmetry. The relatively strong covalent bonds formed between the cations

Materials
Views
www.MaterialsViews.com

ADVANCED
MATERIALS
www.advmat.de

COMMUNICATION

Figure 1. Crystal structure of ZBO. Each $[B_{24}O_{48}]$ sodalite cage is constructed from 24 $[BO_4]$ tetrahedra corner-shared by O_2 atoms, and four $[ZnO_4]$ tetrahedra are locked in the cage by sharing the O_1 atoms located at the center. To explicitly display the sodalite cages, the neighboring boron atoms are connected by thick black lines. Zinc, boron, and oxygen atoms are represented by blue, green, and red balls, respectively. $[ZnO_4]$ tetrahedra are represented by yellow polyhedra and two $[BO_4]$ tetrahedra are represented as an example by Indianred polyhedra at the right upper corner.

and the corner-sharing oxygen atoms would effectively affect the rotation between the rigid B–O groups, hence decreasing the thermal expansion. Guided by this idea, in this work, we screened all borates with cubic structures in the inorganic crystal structure database (ICSD, 2015-1, Version 1.9.6, by Fachinformationszentrum Karlsruhe, Germany) and discovered that $Zn_4B_6O_{13}$ (ZBO) satisfies this structural condition and exhibits an isotropic near-ZTE behavior from 13 to 270 K. Meanwhile, this crystal has high optical transmission in the spectrum range from the ultraviolet, to the visible to near-infrared region and possesses good physicochemical properties for practical applications.

ZBO is crystallized in the cubic *I-43m* space group[21] and exhibits an interesting sodalite cage (β-cage) structure,[21] which is very rare in all known borates. As depicted in **Figure 1**, each sodalite cage is constructed from 24 $[BO_4]$ groups by sharing the corner oxygen atoms (O_2). The $[BO_4]$ groups are interconnected to form B4 quadrangles and B6 hexagons, and six B4 quadrangles and eight B6 hexagons are further connected to construct a close $[B_{24}O_{48}]$ cage with the truncated octahedral shape, i.e., the sodalite cage. In a $[B_{24}O_{48}]$ truncated octahedron, four $[ZnO_4]$ tetrahedra form a radial $[Zn_4O_{13}]$ cluster by sharing the same oxygen atoms (O_1) at the center of the cage. In ZBO, the $[B_{24}O_{48}]$ sodalite cages are fixed by the inside $[Zn_4O_{13}]$ clusters via the relatively strong Zn–O covalent bonds.

The thermal expansion behavior of ZBO between 13 and to 270 K was studied by variable-temperature X-ray diffraction (XRD). In the measured temperature range, no new peaks appeared in all the XRD patterns (Figure S1, Supporting Information), indicating that the structure of ZBO is kept in the cubic *I-43m* space group, and the thermal expansion must be completely 3D isotropic. The crystal structure is refined by the Rietveld method (the refinement plots are listed in Figure S2, Supporting Information),[22] and the variation of the refined cell parameters as the function of temperature is plotted in **Figure 2** (the cell parameters are listed in Table S1 in the Supporting Information). Clearly, the cell parameter of ZBO increases by just 0.03% (from 7.473 to 7.475 Å) from 13 to 270 K, and the fitted average thermal expansion coefficient by PASCal software[23] in the whole temperature range is 1.00(12)/MK. This thermal-expansion behavior is very low, which is also confirmed by the observation that the positions of the XRD peaks (e.g., the (004) peaks shown in the insert in Figure 2) remain nearly constant in the varying temperature environment. The thermal expansion of ZBO is comparable to the thermal expansion of other ZTE materials such as $Fe[Co(CN)_6]$ (−1.47(1)/MK, 4.2 to 300 K),[9] TaO_2F (0.6/MK, 200 to 773 K),[9,10] and $N(CH_3)_4CuZn(CN)_4$ (0.67(11)/MK, 200 to 400 K).[4] In particular, in the temperature range from 13 to 110 K, the thermal expansion coefficient in ZBO is even much smaller (0.28(06)/MK), and can be accurately cataloged to ZTE.[2,4,9,10] It should be noted that the ZTE behavior in ZBO may also extend into the lower temperatures than 13 K, but is not measured in this study due to the limits of the measurement apparatus.

The thermal expansion behavior of materials is closely related to the excitation of lattice vibrations.[24] The volume of the unit cell of ZBO is determined exclusively by the $[B_{24}O_{48}]$ sodalite cage. To elucidate the low thermal expansion of ZBO, we performed a first-principles vibrational analysis, which has
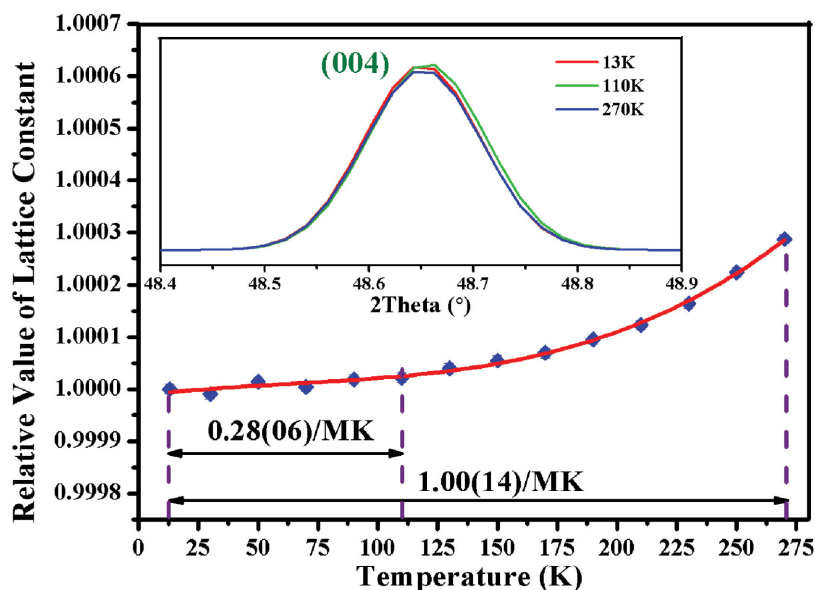

Figure 2. Variation of the refined cell parameters of ZBO with respect to temperature. The inset displays the evolution of the cubic (004) peak Bragg reflection as the temperature changes, the peaks of Kα2 have been removed by Gaussian peak-fitting.

been successfully used to investigate to the mechanism of anomalous-thermal-expansion behavior.[24,25] The phonon spectrum and phonon density of states in the Brillouin zone are displayed in Figure S3 in the Supporting Information. Although the energy dispersion of each phonon branch exists, the modes at the same branch share the similar vibrational property.[24] Thus, we select the modes at Γ-point as the representatives to investigate the low-thermal-expansion mechanism in ZBO. The veracity of the Γ-point analysis is demonstrated by the good agreement between experimental and calculated Raman spectra in Figure S4 in the Supporting Information, and a similar mechanism analysis was also adopted for the famous NTE material ZrW_2O_8.[24] A unit cell of ZBO contains 46 atoms, resulting in 138 degrees of freedom at the Γ-point in the Brillouin zone. The irreducible representation of *I-43m* space group at the Γ-point yields a sum of $20E+45T1+63T2+7A1+3A2$ phonon modes (Table S2, Supporting Information). The thermal behavior of materials under low temperature is widely known to be determined mainly by the phonon modes at low frequencies. The vibrational analysis reveals that with increasing frequency the phonon modes experience an evolution following three types of atomic vibrations. In type I vibrations (from phonon mode 1 to 27, Mode I in **Figure 3** and Video S1 in the Supporting Information), the phonon modes are predominantly attributed to the transverse vibration of Zn atoms. Meanwhile, the $[B_{24}O_{48}]$ sodalite cages remain almost still and therefore contribute little to the thermal expansion. In type-II vibrations (from phonon mode 28 to 78, Mode II in Figure 3 and Video S2 in the Supporting Information), the vibrational modes are assigned mainly to the rotating vibrations between the rigid $[BO_4]$ tetrahedra in the $[B_{24}O_{48}]$ truncated octahedra. These modes are related to the slight breathing vibration of the $[B_{24}O_{48}]$ sodalite cage and contribute to the very small amount

of thermal expansion in ZBO. It should be noted that the contribution of $[BO_4]$ rotations to the thermal expansion in ZBO is some different with that of the rotations between $[WO_4]$ and $[ZrO_6]$ polyhedra in ZrW_2O_8.[26] In ZrW_2O_8, ∠Zr–O–W angles are close to 180°, and the rotations between the rigid $[WO_4]$ tetrahedra and $[ZrO_6]$ octahedra lead to the shortening of W–Zr distances and contraction in volume with increasing temperature (i.e., NTE).[26] In comparison, the ∠B–O–B angles between the $[BO_4]$ tetrahedra in ZBO are just about 130°, and, with increasing temperature, the angles tend to be large, leading to the positive thermal expansion in volume. However, due to the restriction of the relatively strong Zn–O bonds, the opening of ∠B–O–B angle is tiny, so the thermal expansion is still low. In type-III vibrations (from phonon mode 79 to 138, Mode III in Figure 3 and Video S3 in the Supporting Information), these phonon modes are related mainly to the stretching tendency of B–O bonds, which make a major contribution to the thermal expansion at high temperature.

The refined ZBO crystal structures also show that over the temperature range from 13 to 270 K the B–O and Zn–O_1 bond lengths remain almost constant. Meanwhile, the ∠B–O_2–B angles in the $[B_{24}O_{48}]$ cage are opened just about 0.1° (from 127.196° to 127.299°) with the Zn–O_2 bonds slightly stretched approximately 0.004 Å (from 1.959 to 1.963 Å), as displayed in Figure S5 in the Supporting Information. These static structural variations correspond to the atomic vibrations of the vibration types Mode I and II. Therefore, the low thermal expansion in ZBO originates from the following mechanism: at low temperatures (below 110 K), the atomic vibrations of the $[B_{24}O_{48}]$ sodalite cage are hardly stimulated, and ZBO remains almost constant in volume. With increasing temperature (from 110 to 270 K), the rotations between the $[BO_4]$ tetrahedra are gradually triggered, but these rotation are restricted by the relatively
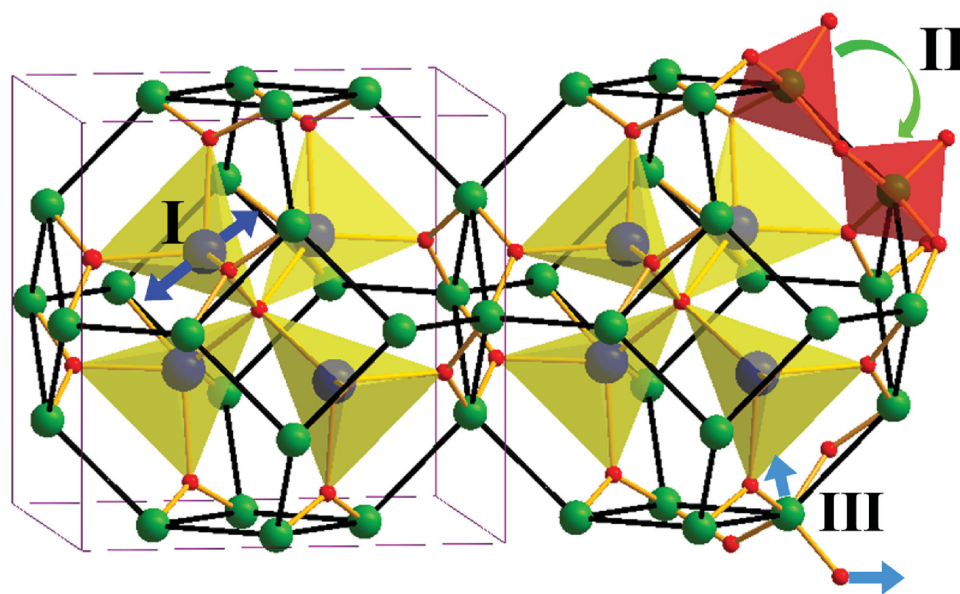
Figure 3. Schematic of the dominant atomic vibrations for the phonon modes. Mode I: stretching of $[ZnO_4]$ tetrahedra from phonon modes 1 to 27, Mode II: rotating of $[BO_4]$ tetrahedra from phonon modes 28 to 78, and Mode III: stretching of B–O bond from phonon modes 79 to 138. The zinc, boron, and oxygen atoms are represented by blue, green, and red balls, respectively. $[ZnO_4]$ tetrahedra are represented by yellow polyhedra and two $[BO_4]$ tetrahedra are represented as an example by Indianred polyhedra at the right upper corner.

strong Zn–O bonds, ZBO therefore exhibits a slight thermal expansion. As the temperature increases further (above 270 K), with the weakening of Zn–O bonds, the rotation of the [BO$_4$] tetrahedra is enhanced. Meanwhile, the B–O bonds are gradually undergoing stretching, so the thermal expansion in ZBO exhibits a tendency to increase (3.5/MK at room temperature.[27]) Interestingly, the mechanism of low thermal expansion in ZBO is different from that in other ZTE materials, e.g., in Fe[Co(CN)$_6$], N(CH$_3$)$_4$CuZn(CN)$_4$ and TaO$_2$F. The ZTE behaviors of Fe[Co(CN)$_6$] and N(CH$_3$)$_4$CuZn(CN)$_4$ mainly originate from the balancing effect between transversal vibration and positive thermal expansion,[4,9] while in TaO$_2$F this effect is mainly attributed to the local distortions away from the ideal ReO$_3$-type structure lead by anion site disorder.[28]

ZBO is congruently melting (Figure S6, Supporting Information) and exhibits good growth habit. It is relatively easy to obtain bulk single crystals using the conventional top-seeded growth method. Using the flux of pre-synthesized polycrystals, we grew large-sized ZBO single crystals exhibiting a very good optical quality with dimensions of ≈40 mm × 40 mm × 18 mm, as displayed in **Figure 4**a and Figure S7 in the Supporting Information. At the same time, during the growth process no oxygen-free atmosphere is needed, and no toxic ingredients are introduced. The easy growth and environmentally friendly habits are very beneficial for the practical applications of ZBO.

The optical transmittance measurements (Figure 4b) show that ZBO has a very high transparency covering a wide region from the UV, to the visible, to the near-infrared (wavelength from 217 to 3100 nm). The UV absorption edge of ZBO (217 nm, corresponding to the bandgap of 5.73 eV) is the shortest ever reported among the ZTE crystals. The measured bandgap is in very consistent with the first-principles result with the calculated bandgap of 5.55 eV. The ab initio partial density of states (see Figure S8 in the Supporting Information) reveals that the electronic energy levels near the forbidden band are composed predominantly of the zinc and oxygen orbitals, indicating that the bandgap of ZBO is determined mainly by the electron transition within the Zn–O bonds. Due to the relatively strong electronegativity of the zinc atoms, the Zn 3d orbitals hybridize strongly with the O 2p orbital between −10 and 0 eV.

The strong hybridization over a large energy range of these orbitals can effectively decrease the energy of the valence bands and thus expand the crossing energy (i.e., bandgap) of the electron transition from the valence bands to the conduction bands.

The thermal stability, thermal conductivity, and mechanical hardness of ZBO have been investigated. Differential scanning calorimetry (DSC) measurements reveal that no endothermic peak appears below the melting point (1272 K), indicating the very good thermal stability of ZBO (Figure S9 in the Supporting Information). Meanwhile, ZBO possesses very good thermal conducting properties and is superior to majority of the borates. For example, the thermal-conduction coefficient (κ) of ZBO is 30.54 W m^{-1} K^{-1} at 298 K (Table S3, Supporting Information), which is larger than that of BBO (κ_c = 1.64 W m^{-1} K^{-1}, Popov et al.[29]) and LBO ($\kappa_{average}$ = 3.50 W m^{-1} K^{-1}, Grechin et al.[30]) at the same temperature by approximately one order of magnitude. From the viewpoint of optical applications, the high thermal conductivity can effectively eliminate the accumulation of thermal stress. Coupled with the wide bandgap, the optical damage threshold in ZBO would be significantly improved. In addition, the Vickers hardness of ZBO is 1304, which is slightly larger than the Vickers hardness of quartz (1260).[31] The high mechanical strength enables the use of ZBO in harsh environments. Benefiting from the good optical, thermal, and mechanical properties, ZBO could find important applications in many high-precision optical instruments used at low temperatures (especially under liquid-nitrogen conditions), such as ultracold optical scanners, optical space telescopes, and optical fiber temperature transducers for low-temperature measurements.

In conclusion, intrinsic isotropic near-ZTE behavior has been discovered in ZBO, as the first case in borates. First-principles calculations demonstrate that the very low thermal expansion originates mainly from the invariability of the solid [B$_{24}$O$_{48}$] truncated octahedra fixed by the [Zn$_4$O$_{13}$] clusters in the ZBO structure. Optical transmittance measurements show that the transmission range of ZBO covers a wide spectral region from the UV, to the visible, to the near-infrared, and the UV cutoff edge is the shortest among the congeners, which also stems from the relatively strong Zn–O bond. Meanwhile, ZBO exhibits good single-crystal growth, high thermal stability and
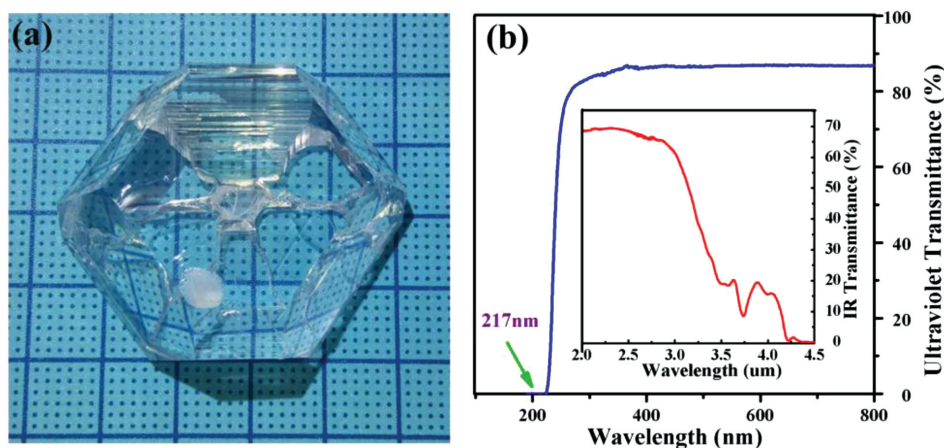
Figure 4. a) As-grown bulk ZBO single crystal (≈40 mm × 40 mm × 18 mm). b) UV–vis transmission spectrum of ZBO. The inset displays the IR transmission spectrum.

COMMUNICATION

thermal conductivity, and high mechanical hardness. The discovery presented in this work adds one important member to the small family of ZTE materials. More importantly, the present study revives the studies on new functionalities in borates, which have long been overlooked, and may eventually lead to discoveries of more exciting and exotic emerging physicochemical properties in borates.

Supporting Information

Supporting Information is available from the Wiley Online Library or from the author.

Acknowledgements

[1] a) A. Sleight, *Nature* **2003**, *425*, 674; b) P. Lama, R. K. Das, V. J. Smith, L. J. Barbour, *Chem. Commun.* **2014**, *50*, 6464.

[2] J. Chen, L. Hu, J. Deng, X. Xing, *Chem. Soc. Rev.* **2015**, *44*, 3522.

[3] a) S. E. Tallentire, F. Child, I. Fall, L. Vella-Zarb, I. R. Evans, M. G. Tucker, D. A. Keen, C. Wilson, J. S. O. Evans, *J. Am. Chem. Soc.* **2013**, *135*, 12849; b) X. Song, Z. Sun, Q. Huang, M. Rettenmayr, X. Liu, M. Seyring, G. Li, G. Rao, F. Yin, *Adv. Mater.* **2011**, *23*, 4690.

[4] A. E. Phillips, G. J. Halder, K. W. Chapman, A. L. Goodwin, C. J. Kepert, *J. Am. Chem. Soc.* **2010**, *132*, 10.

[5] a) J. P. Attfield, *Nature* **2011**, *480*, 465; b) X. Y. Shen, C. Viney, E. R. Johnson, C. C. Wang, J. Q. Lu, *Nat. Chem.* **2013**, *5*, 1035.

[6] a) L. Hu, J. Chen, L. Fan, Y. Ren, Y. Rong, Z. Pan, J. Deng, R. Yu, X. Xing, *J. Am. Chem. Soc.* **2014**, *136*, 13566; b) K. J. Miller, C. P. Romao, M. Bieringer, B. A. Marinkovic, L. Prisco, M. A. White, *J. Am. Ceram. Soc.* **2013**, *96*, 561.

[7] O. Volkova, Y. Arango, N. Tristan, V. Kataev, E. Gudilin, D. Meier, T. Lorenz, B. Buchner, A. Vasil'ev, *JETP Lett.* **2005**, *82*, 444.

[8] T. Kiyama, K. Yoshimura, K. Kosuge, Y. Ikeda, Y. Bando, *Phys. Rev. B* **1996**, *54*, R756.

[9] S. Margadonna, K. Prassides, A. N. Fitch, *J. Am. Chem. Soc.* **2004**, *126*, 15390.

[10] J. Z. Tao, A. W. Sleight, *J. Solid State Chem.* **2003**, *173*, 45.

[11] J. R. Salvador, F. Gu, T. Hogan, M. G. Kanatzidis, *Nature* **2003**, *425*, 702.

[12] C. P. Romao, F. A. Perras, U. Werner-Zwanziger, J. A. Lussier, K. J. Miller, C. M. Calahoo, J. W. Zwanziger, M. Bieringer, B. A. Marinkovic, D. L. Bryce, M. A. White, *Chem. Mater.* **2015**, *27*, 2633.

[13] a) T. Legero, T. Kessler, U. Sterr, *J. Opt. Soc. Am. B* **2010**, *27*, 914; b) P. Riello, P. Canton, N. Comelato, S. Polizzi, M. Verita, G. Fagherazzi, H. Hofmeister, S. Hopfe, *J. Non-Cryst. Solids* **2001**, *288*, 127; c) H. Duncker, O. Hellmig, A. Wenzlawski, A. Grote, A. J. Rafipoor, M. Rafipoor, K. Sengstock, P. Windpassinger, *Appl. Opt.* **2014**, *53*, 4468; d) H. Bach, D. Krause, *Low Thermal Expansion Glass Ceramics*, Springer, Berlin/Heidelberg, Germany **2005**, p. 121.

[14] C. T. Chen, T. Sasaki, R. K. Li, Y. C. Wu, Z. S. Lin, Y. Mori, Z. G. Hu, J. Y. Wang, G. Aka, M. Yoshimura, Y. Kaneda, *Nonlinear Optical Borate Crystals-Principles and Applications*, Wiley-VCH, Weinheim, Germany **2012**.

[15] R. S. Bubnova, S. K. Filatov, *Z. Kristallogr.* **2013**, *228*, 395.

[16] R. S. Bubnova, S. K. Filatov, *Phys. Status Solid B* **2008**, *245*, 2469.

[17] X. Jiang, S. Luo, L. Kang, P. Gong, W. Yao, H. Huang, W. Li, R. Huang, W. Wang, Y. Li, X. Li, X. Wu, P. Lu, L. Li, C. Chen, Z. Lin, *Adv. Mater.* **2015**, *27*, 4851.

[18] W. Yao, X. Jiang, R. Huang, W. Li, C. Huang, Z. Lin, L. Li, C. Chen, *Chem. Commun.* **2014**, *50*, 13499.

[19] Y. Lou, D. Li, Z. Li, S. Jin, X. Chen, *Sci. Rep.* **2015**, *5*, 10996.

[20] R. S. Bubnova, N. K. Stepanov, A. A. Levin, S. K. Filatov, P. Paufler, D. C. Meyer, *Solid State Sci.* **2004**, *6*, 629.

[21] P. Smith, L. Rivoir, S. Garciablanco, *An. R. Soc. Esp. Fis. Quim.* **1961**, *57A*, 263.

[22] H. M. Rietveld, *J. Appl. Crystallogr.* **1969**, *2*, 65.

[23] M. J. Cliffe, A. L. Goodwin, *J. Appl. Crystallogr.* **2012**, *45*, 1321.

[24] V. Gava, A. L. Martinotto, C. A. Perottoni, *Phys. Rev. Lett.* **2012**, *109*, 195503.

[25] a) F. Wang, Y. Xie, J. Chen, H. Fu, X. Xing, *Appl. Phys. Lett.* **2013**, *103*, 221901b; b) J. W. Zwanziger, *Phys. Rev. B* **2007**, *76*, 052102.

[26] A. K. A. Pryde, K. D. Hammonds, M. T. Dove, V. Heine, J. D. Gale, M. C. Warren, *J. Phys.: Condens. Matter.* **1996**, *8*, 10973.

[27] L. Bohaty, S. Haussuhl, J. Liebertz, S. Stahr, *Z. Kristallogr.* **1982**, *161*, 157.

[28] C. R. Morelock, B. K. Greve, M. Cetinkol, K. W. Chapman, P. J. Chupas, A. P. Wilkinson, *Chem. Mater.* **2013**, *25*, 1900.

[29] P. A. Popov, N. V. Moiseev, A. E. Kokh, K. A. Kokh, *Inorg. Mater.* **2011**, *47*, 163.

[30] S. G. Grechin, A. V. Zuev, A. E. Kokh, N. V. Moiseev, P. A. Popov, A. A. Sidorov, A. S. Fokin, *Quantum Electron.* **2010**, *40*, 509.

[31] Properties of silicon dioxide in http://www.memsnet.org/material/silicondioxidesio2bulk/, (accessed: June 2016).